JOURNAL OF MASS SPECTROMETRY
J. Mass Spectrom. 2004; **39**: 361–367
Published online 3 February 2004 in Wiley InterScience (www.interscience.wiley.com). DOI: 10.1002/jms.592

JMS

Peak capacity of ion mobility mass spectrometry: the utility of varying drift gas polarizability for the separation of tryptic peptides

Brandon T. Ruotolo, John A. McLean, Kent J. Gillig and David H. Russell*

Laboratory for Biological Mass Spectrometry, Department of Chemistry, Texas A&M University, College Station, Texas 77843, USA

Received 21 July 2003; Accepted 25 November 2003

Ion mobility mass spectrometry (IM-MS) peptide mass mapping experiments were performed using a variety of drift gases (He, N_2, Ar and CH_4). The drift gases studied cover a range of polarizabilities ($(0.2–2.6) \times 10^{-24}$ cm^3) and the peak capacities obtained for tryptic peptides in each gas are compared. Although the different gases exhibit similar peak capacities (5430 (Ar) to 7580 (N_2)) in some cases separation selectivity presumably based on peptide conformers (or conformer populations), is observed. For example the drift time profiles observed for some tryptic peptide ions from aldolase (rabbit muscle) show a dependence on drift gas. The transmission of high-mass ions ($m/z > 2000$) is also influenced by increased scattering cross-section of the more massive drift gases. Consequently the practical peak capacity for IM-MS separation cannot be assumed to be solely a function of resolution and the ability of a gas to distribute signals in two-dimensional space; rather, peak capacity estimates must account for the transmission losses experienced for peptide ions as the drift gas mass increases. Copyright © 2004 John Wiley & Sons, Ltd.

KEYWORDS: proteomics; matrix-assisted laser desorption/ionization; separation; peptides; conformation

INTRODUCTION

Current efforts in medicinal chemistry,[1] cellular biology[2] and structural biology[3] rely heavily on rapid, sensitive, mass spectrometry-based methods for analyte identification. Although substantial progress has been made in the development of mass spectrometry for the analysis peptides and proteins,[4] there are still several areas where additional improvements are needed. For example, mass spectra of highly complex samples that contain multiple classes of analytes (e.g. the contents of a typical cell) are often too complex to manually interpret, necessitating the continued development of computer-assisted database search algorithms.[5] In addition, the simultaneous ionization of such a wide range of compounds often leads to increased suppression of certain analyte species, effectively decreasing the dynamic range.[6] The latter effect has been mitigated to some degree through the use of liquid-phase separation prior to mass analysis,[7] and several groups have successfully utilized liquid chromatography/mass spectrometry (LC/MS) methods to interrogate a wide array of complex samples.[8–10] On the other hand, the disparate time-scales of LC, which requires minutes to hours for analyte separation, and time-of-flight (TOF) MS, which requires only a few microseconds to acquire the entire mass spectrum, results in an analytical technique that inefficiently utilizes the throughput capacity of TOF instruments.[11]

Currently, ion mobility (IM) separation methods are becoming increasingly popular for both complex mixture analysis and structural determinations of gas-phase ions. This increased interest in IM as a structural probe of gas-phase ions is due to recent work by the groups of Bowers,[12] Jarrold[13] and Clemmer.[14,15] On the other hand, our laboratory has emphasized the utility of IM-TOFMS for high-throughput peptide mass mapping,[16] screening protein digests for post-translationally modified peptides[17] and the development of highly parallel peptide sequencing methodologies.[18,19]

IM separations are typically conducted on the millisecond time-scale, and drift times are directly related to the collision cross-section of the analyte ions. IM separations on the millisecond time-scale are ideally suited to TOFMS, which requires microseconds to acquire a single mass spectrum. Our laboratory achieves high time-bin resolution (typically ~2 μs) in the IM separation by utilizing a series of spectra, progressively delayed from the start trigger, which are then reconstructed (interleaved) into a complete plot of drift time vs m/z.[20] For applications in peptide mass mapping, the speed and conformational selectivity of IM are typically offset

*Correspondence to: David H. Russell, Laboratory for Biological Mass Spectrometry, Department of Chemistry, Texas A&M University, P.O. Box 30012, College Station, Texas 77843, USA.
E-mail: russell@mail.chem.tamu.edu
Contract/grant sponsor: National Science Foundation;
Contract/grant number: CHE-9629966.
Contract/grant sponsor: Department of Energy, Division of Chemical Sciences; Contract/grant number: DE-FG03-95ER14505.
Contract/grant sponsor: Texas Advance Research Program/Advanced Technology Program; Contract/grant number: TARP/ATP 010366-0064-2001.

by the high correlation between drift time (cross-section) and mass for a particular molecular class (e.g. peptides), and limits the theoretical peak capacity (ϕ) of the technique for a series of singly charged peptide ions to $\sim 1 \times 10^3 - 1 \times 10^4$.[21]

Structural studies utilizing IM and the majority of IM peptide separations[13,14] have been carried out in He drift gas, owing to its low scattering cross-section (leading to increased transmission efficiency) and low polarizability, which simplifies the extraction of structural information from collision cross-section measurements. Several groups have introduced additional selectivity to mobility separation through the use of drift gases that possess a higher degree of polarizability than He. For example, Hill and co-workers utilized Ar, N_2, CO_2 and SF_6 to effect changes in selectivity for the gas-phase separation of anilines, amines, illicit drugs and small peptides ions (approaching m/z 500).[22–25] For all drift gases other than He, significant ion–induced dipole interactions are introduced into the separation, thus necessitating the treatment of the collision cross-section as a combination of hard-sphere collisions (a geometry-driven parameter) and interaction potentials that develop between the ion and the neutral collision partners (a parameter driven by the chemistry of the analyte). This type of ion–induced dipole interaction has been well characterized in the literature and has been mathematically described by Mason and McDaniel[26,27] as

$$K_{\text{pol}} \equiv \frac{13.853}{(\alpha_{\text{p}}\mu)^{1/2}} \quad (1)$$

where α_{p} is the polarizability (in Å^3), μ is the reduced mass and K_{pol} (the mobility contribution due to polarizability alone) approaches K_0 (reduced mobility) as the temperature of the system and energy of the collisions approach zero. Equation (1) is often referred to as the polarization limit, and has been used successfully to interpret the contribution of ion–induced dipole interaction to the mobility of atomic and small molecule ions.[28] This expression predicts a sharp decrease in the influence of ion–induced dipole on the collision cross-section, approaching zero for ions that exceed 500 u.[29,30]

This paper describes our efforts to increase the peak capacity of peptide separation for IM-MS methodologies by using drift gases that possess a higher degree of polarizability than helium. The data presented here indicate that there is no observable effect of drift gas on the relative mobility of peptide ions of m/z 500–3500, and this is consistent with predictions based on Eqn (1) and previous experiments.[27] On the other hand, drift time profiles for some peptide sequences are observed to change as a function of drift gas, suggesting that some conformational selectivity can be achieved through an increase in ion–neutral interaction, an observation that is supported by recent experiments by Kohtani and Jarrold.[31] In addition, the number of observable peptide signals changes as a function of drift gas, allowing the ϕ values reported here to reflect complex issues such as signal suppression and peptide fragment production.

EXPERIMENTAL

Ion mobility instrumentation

The matrix-assisted laser desorption/ionization (MALDI)–ion mobility (IM)–orthogonal time-of-flight mass spectrometer (o-TOFMS) used in these studies consists of a MALDI ion source (N_2 laser, 337 nm) situated at one end of a periodic focusing ion mobility drift cell (typical resolution for peptides $\sim$50–60 $t/\Delta t$).[32] Ions are created at the operating pressure of the 30 cm drift cell (in these experiments 0.660 Torr (1 Torr = 133.3 Pa) of ultra-high purity He, N_2, CH_4, or Ar) and are pulled electrostatically through the drift cell using a field strength of $\sim$85 V cm^{-1} Torr^{-1}. The drift cell pressure was monitored with a capacitance manometer (Inficon, Balzers, Liechtenstein). Upon elution from the drift cell, ions are sampled by a 30 cm TOFMS instrument, capable of $\sim$200 mass resolution ($m/\Delta m$). Two-dimensional (2-D) data are acquired using a custom software package (developed by T. Egan, Ionwerks, Houston, Texas) and analysis (peak picking/visualization) is performed with the Transform software package (IDL, Boulder, CO, USA).

Sample preparation

Single-component protein samples (Sigma, St. Louis, MO, USA) are thermally denatured and digested with sequencing-grade modified trypsin (Promega, Madison, WI, USA) according to protocols detailed previously.[33] Unless noted, otherwise the proteins used in this study are cytochrome *c* (horse heart), myoglobin (horse heart), α-casein (bovine), β-casein (bovine), hemoglobin (bovine), transferrin (bovine), serum albumin (bovine), ubiquitin (bovine), carbonic anhydrase (bovine), ribonuclease A (bovine), phosphorylase (rabbit muscle), aldolase (rabbit muscle), ovalbumin (chicken egg white), lysozyme (chicken egg white), and luciferase (marine bacterium *Vibrio harbeyi*). A 5 µl volume of each digest was diluted to a 2000 : 1 matrix to analyte ratio with α-cyano-4-hydroxycinnamic acid and spotted on the MALDI sample probe without further purification or preparation.

Peak capacity calculations

The peak capacity of an IM-MS separation is calculated using a method outlined in previous work.[21] Briefly, the deviation from a linear fit for a large dataset of peptides is used to establish the width of 2-D separation space on the drift time axis, as illustrated in Plate 1. The mass range utilized for these calculations is m/z 500–3500, a typical range for peptide ions resulting from tryptically digested proteins. The area of the separation space is calculated (in peaks) using average resolution values for both axes, 50 ($t/\Delta t$, at full width at half-maximum (FWHM)) for the drift time axis and 200 ($m/\Delta m$, FWHM) for the mass axis. The peak capacity then corresponds to the maximum theoretical number of individual peaks, or components, that can be distinguished by a separation method.[34]

RESULTS AND DISCUSSION

The goal of this study was to estimate the capability of IM-MS relative to other separation strategies for the analysis of complex peptide mixtures. We chose to use peak capacity

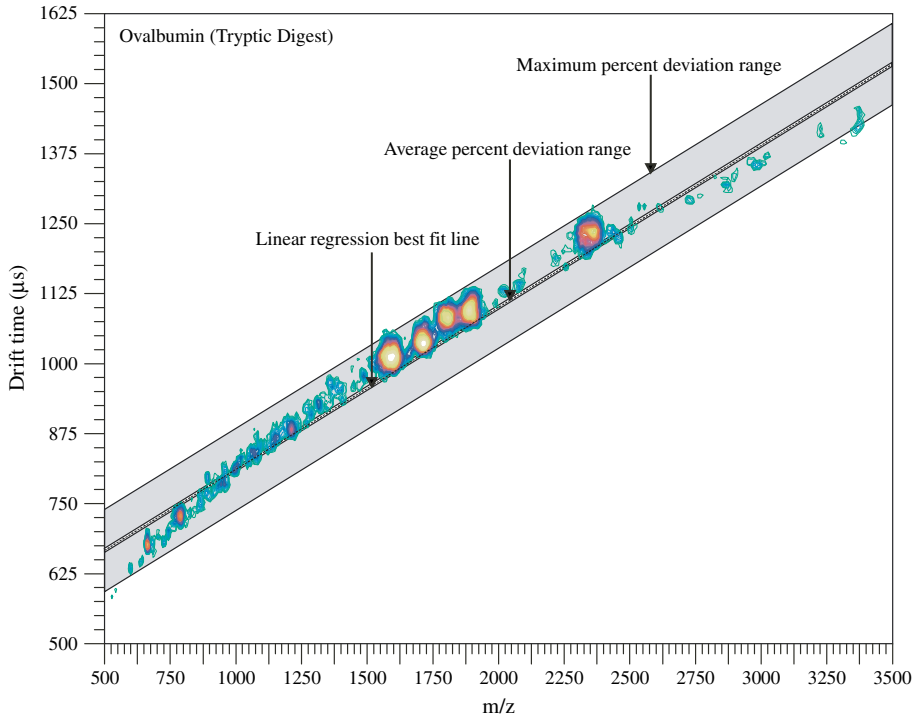

Plate 1. A drift time–*m*/*z* plot of a tryptic digest of ovalbumin (chicken egg white) utilizing methane as a drift gas. Overlaid are schematic representations of the separation regions defined in this paper (see text) and the linear regression best-fit line for the data.

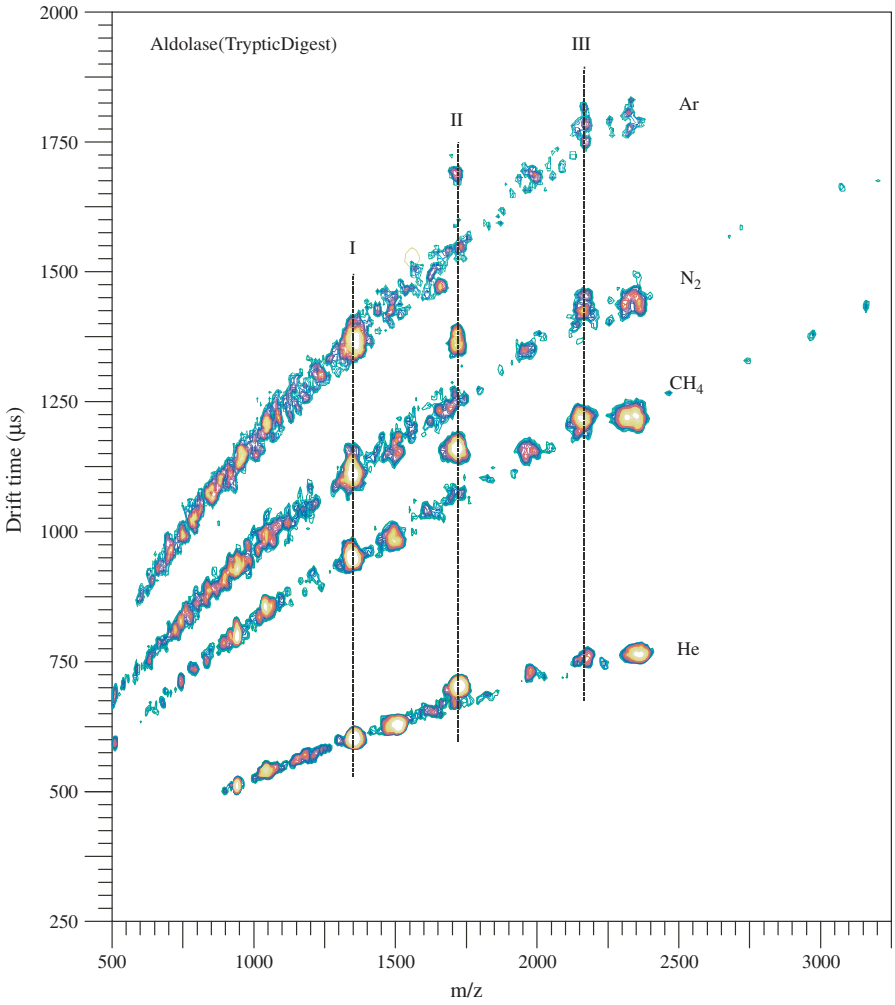

Plate 2. Four overlayed drift time vs *m*/*z* plots for a tryptic digest of aldolase (rabbit muscle), for each of the drift gases utilized (Ar, N_2, CH_4 and He). Three peptides signals (**I, II**, and **III**) are labeled and discussed in the text. Vertical dashed lines are added to guide the eye.

as an indication of the effectiveness of such an experiment, because it is a measurement of the complexity of samples that can be theoretically analyzed by a separation method.[35] Although the previous dataset exhibited a relatively high correlation to a linear relationship between drift time and m/z (0.998),[21] a poorer correlation coefficient was obtained for the data presented here (0.98). The observed curvature is a consequence of multiple factors: the low pressures and high field strengths required for data acquisition over a variety of drift gases with the current instrumentation,[32] and the observation of peptide fragments over a larger mass range than analyzed in our previous study.[21] The linear fit utilized in the peak capacity calculations in this study, and utilized previously,[21] accounts for the high degree of correlation between collision cross-section (represented in the drift time dimension) and mass for a homologous series of ions. Furthermore, basing the calculation on a linear relationship, rather than a more complex polynomial function,[36] minimizes computational complexity while retaining an accurate estimate of the theoretical peak capacity. Plate 1 illustrates a typical separation of peptides by IM-MS. To estimate peak capacity, first a linear regression is performed on the dataset (centered within the black-shaded region of Plate 1). Based on a residuals analysis of the least-squares regression, two separation spaces are defined: (1) the area inscribed by the average percent deviation of peptides for the best fit line (shown in black), and (2) the area described by the maximum deviation (or 'range') of all peptides in the dataset (shown in gray). The peak capacity is then calculated for both regions. Peak capacity estimations performed using the maximum spread of the data are likely to be an overestimate of the true peak capacity (because our data indicate that a small number of signals will populate the extreme regions of this space), whereas calculations utilizing the average spread of the data are likely to underestimate the peak capacity of IM-MS (because this space does not accurately account for the total spread of our dataset). Here, both numbers are reported in an effort to present more accurately the peak capacity of IM-MS, which lies between the estimates using the average deviation and the maximum spread observed.

Figure 1 summarizes data for the entire dataset of 1212 peptides in terms of deviation from a linear relationship between drift time and m/z. The residual plot of all peptide ion signals (Fig. 1(A)), is independent of origin (i.e. protein) and drift gas (He, CH_4, N_2 or Ar), and sorted according to deviation from a linear fit. It is important to note that the magnitude of each bar on the y-axis for the residual plot shown in Fig. 1(A) denotes the magnitude of the deviation from a linear fit for a single peptide, while the number on the x-axis denotes the rank/order of that single peptide when the dataset is sorted in terms of the amount of deviation exhibited (y-axis value). The majority of peptide ion signals (676 out of 1212) fall within a single standard deviation from a linear fit between drift time and m/z (expressed as $\pm 1\sigma$ on Fig. 1(A)). More than 95% of all peptide ions fall within $\pm 4\sigma$, and we have suggested that the remaining peptide ions exhibit gas-phase structures (α-helical, β-sheet, etc.) that are distinct from those of the majority of gas-phase peptides (compact random coil).[36] Also observable in Figure 1(A) is

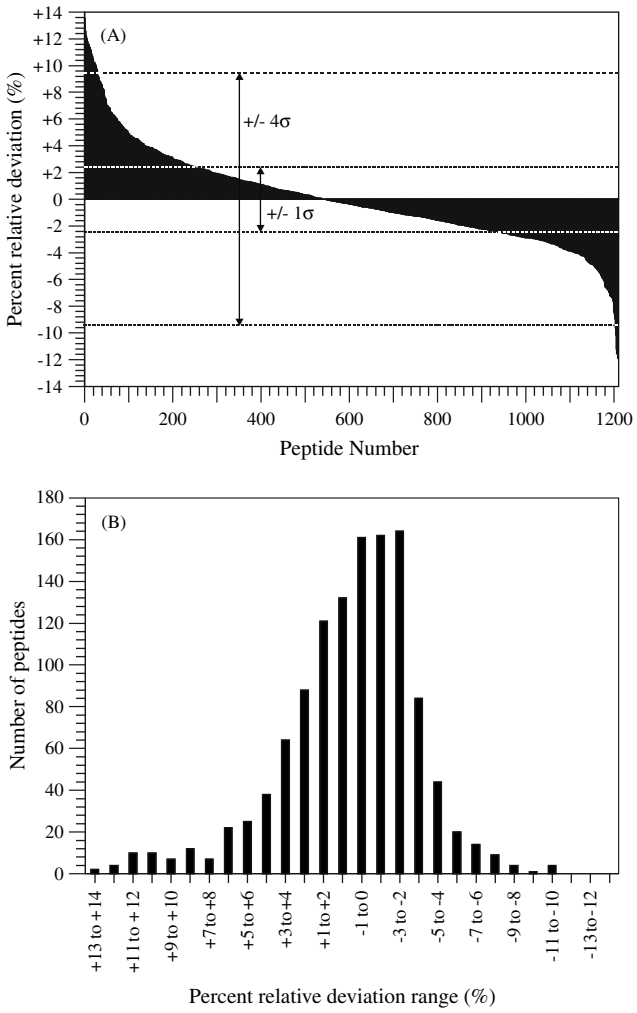

Figure 1. (a) A residual plot, ordered (on the 'peptide number' axis) by the magnitude of the percentage relative deviation (or the deviation of a particular peptide from a linear fit, normalized to the drift experienced by the peptide) from the greatest positive deviation to the greatest negative deviation. The variance of the data is expressed in terms of standard deviation (σ). (b) The same data set as (a), presented as a histogram.

the apparent asymmetry of the dataset, i.e. the dataset is biased towards negative deviation. This is a consequence of fitting a straight line to data points having some degree of curvature, as illustrated in Plate 1. Figure 1(B) further illustrates the bias of this combined dataset towards negative deviation from a strictly linear regression. It is important to note that polynomial fits were initially employed in these calculations in order to account more accurately for the curvature of the data; however, the peak capacities calculated from polynomial fits are only 1.5 times lower than those calculated utilizing a linear approximation (e.g., ϕ is ~5000 peaks for the polynomial fit of the digest data taken in nitrogen drift gas, rather than ~7600). We do not consider a difference of this magnitude significant for estimates of this type.

Figure 2 contains four separate residual plots (similar to Fig. 1(A)) for data acquired in (A) helium, (B) methane, (C) nitrogen and (D) argon. Peptides are ordered within each according to their percentage relative deviation from a linear

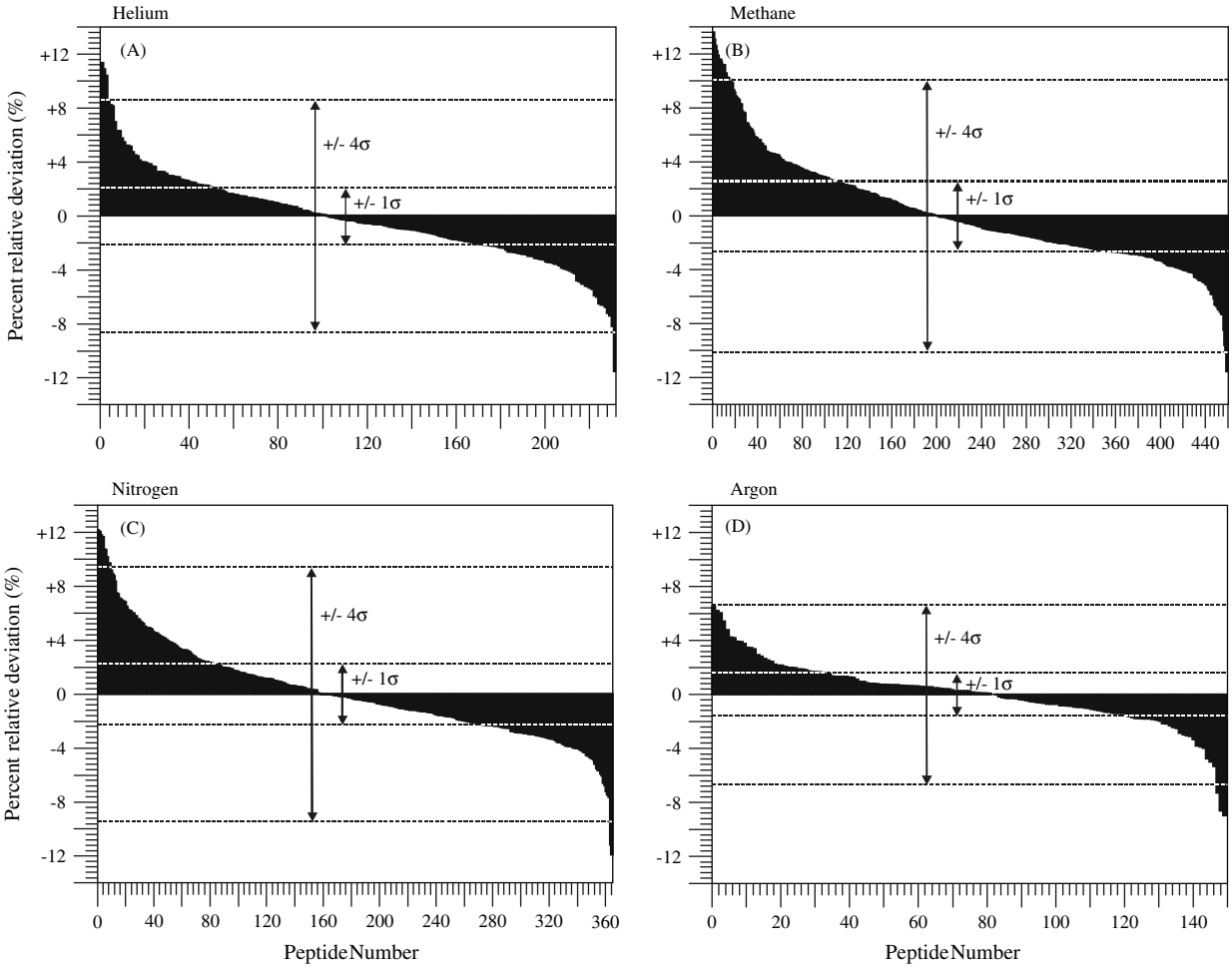

Figure 2. Residual plots, illustrating the deviation of peptides (normalized to the drift experienced by the ion) for each of the four drift gases discussed in this paper: (A) helium, (B) methane, (C) nitrogen and (D) argon. As in Fig. 2(A), the 'peptide number' axis is determined by the magnitude of the normalized deviation experienced for each peptide in each gas.

relationship between m/z and drift time. The helium residual plot (Fig. 2(A)) consists of data from previous work,[21] and was acquired at lower field strength (20–30 V cm^{-1} Torr^{-1}) relative to the other three datasets (80–90 V cm^{-1} Torr^{-1}). The comparison of Fig. 2(A) with Fig. 2(B)– (D) is a valid one, as our data indicate that the peak capacity of IM separation for peptides does not vary significantly as a function of field strength (manuscript in preparation). Deviations in this figure are reported in terms of standard deviation (as in Fig. 1(A)). All four datasets exhibit the same general distributions as the combined dataset presented in Fig. 1(A), with the notable exception of argon. The slight bias toward positive deviation observed for the argon data compared with the other gases is probably due to the lower transmission efficiency of high-m/z ions ($m/z > 2000$) through the more massive buffer gas.

It is also informative to compare the overall deviations of peptide ion signals in drift time as a function of the drift gas used for the separation, i.e. the overall spread in drift time from a linear fit for each dataset. As labeled in Fig. 2, the methane dataset possesses the greatest overall variation from a linear fit, where 1σ corresponds to $\pm 2.56\%$ relative deviation and 4σ corresponds to $\pm 10.24\%$ relative deviation from a linear fit between m/z and drift time. For the argon dataset, the lowest overall variation from a linear fit is observed, where 1σ corresponds to 1.67% and 4σ corresponds to 6.67% relative deviation. In general, these data suggest that the gases are nearly equivalent in their ability to disperse signals in 2-D space. It is important to note that subtle differences, in terms of variance from a strictly linear fit, are observed between the drift gases investigated in these studies. Figure 3 shows a probability density diagram for the mobility separation of peptide ions in each of the four gases utilized in this study created by plotting a normalized percentage of the peptides in each dataset as a function of percentage relative deviation. The normalized percentage axis (y-axis) was calculated by fitting the peptides in each dataset into x-axis bins based on percent relative deviation from a linear fit, converting the numbers into a percentage, and then normalizing to the number of peptides observed in each dataset. Argon exhibits the sharpest probability density for peptide ions, i.e. there is a greater apparent linear correlation between mass and mobility for peptides in argon. As in Fig. 2, this observation can also be explained in terms of differences in the raw data for argon relative to the other three gases. Fewer high-mass digest fragments are observed in argon than in methane, nitrogen or helium, creating a low mass bias in the argon dataset and, thus,

a higher apparent correlation between m/z and drift time, as observed in Fig. 3. In terms of general observation of these datasets, there appears to be little difference between the four gases presented here in terms of mass–mobility correlation, suggesting that the range of polarizabilities ($(0.2–2.6) \times 10^{-24}$ cm^3) utilized in these studies does not enhance the interaction potential between peptide ions and the neutral drift gas. This result appears to contradict to the work of Hill and co-workers, whose data suggest that the selectivity of IM separation can be modified for selected small peptides and organic molecules utilizing drift gases having polarizabilities similar to those used here.[22–24] This can be explained, however, since the peptides studied by Hill and co-workers were less massive ($m/z < 500$) than those used to compile our dataset (m/z 500–3500). In addition, the field strengths used in these studies are 2–5 times higher than those of Hill and co-workers, thereby increasing the relative velocity between ion and neutral, and decreasing the probability of a long-range (i.e. ion–dipole or ion–induced dipole) interaction. On the other hand, we have recently acquired data that indicate that the peak capacity for tryptic peptides in this mass range (m/z 500–3500) is unaffected when utilizing polarizable drift gases at room temperature, and this work will be the subject of a future publication. It is important to note that isolated cases of sequence selectivity as a function of drift gas, if they exist for larger peptides, may not increase our estimates of the peak capacity of peptide separation, as our data suggest that such cases are rare (~1% of the current dataset).

It is also instructive to focus on the differences present in the mass–mobility plot of a single protein tryptic digest as a function of drift gas. Plate 2 contains four overlaid mass–mobility plots for tryptic peptide ions derived from rabbit muscle aldolase, all acquired at equivalent field strengths (80–90 V cm^{-1} Torr^{-1}). As expected, the drift time required to separate peptides increases with the mass of the drift gas used (i.e. increased collision cross-section). Several high-intensity peptide signals common to each individual plot are highlighted as examples of potential conformational selectivity differences as a function of drift gas. In Plate 2, peptide signal **I** (m/z 1342, PHSHPALTPEQK) is used as a control, because the signal does not change appreciably as a function of drift gas. Conversely, the relative abundance for peptide signal **II** (m/z 1693, YSHEEIAMATVTALR) changes in intensity relative to **I**, most notably in the argon data, and the peptide signal at position **III** in Plate 2 (m/z 2108, IGEHTPSALAIMENANVLAR) changes both in intensity relative to **I** and in drift-time profile. In helium drift gas, signal **III** appears to have a single maximum profile in drift time, whereas, in the other three gases **III** appears to have multiple unresolved maxima in the drift time dimension.

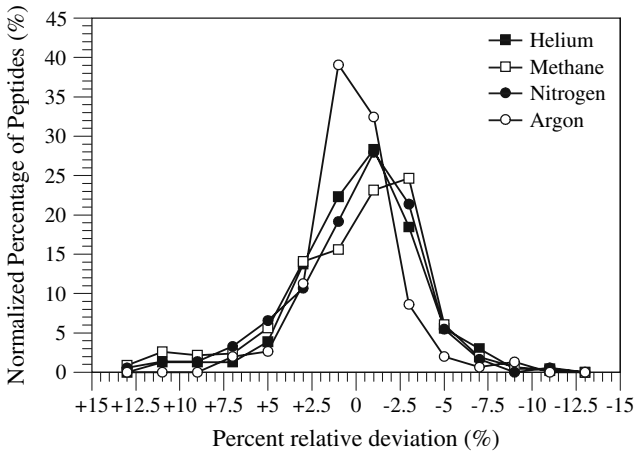

Figure 3. Plot of percentage relative deviation vs normalized percentage of peptides (or the appearance frequency of peptide ion signals possessing the given magnitude of percentage relative deviation). The result is a probability density diagram for the appearance of peptides relative to a linear relationship between drift time and *m/z* for each of the gases discussed in the text.

In an earlier study, we proposed that the signals that are poorly correlated with the average relationship between drift time and m/z for singly charged peptide ions, such as the peptide signal at position **II** in Plate 2, possess a more extended gas-phase structure relative to the majority of tryptic peptides.[37] It is apparent in Plate 2 that the signal at position **II** changes in terms of absolute deviation from the typical peptide signal trend as a function of drift gas by a factor of nearly 4, from 37 μs in helium to 140 μs in argon. However, such an observation does not suggest a change in selectivity as a function of drift gas because the relative (normalized) deviation for this peptide remains unchanged. The larger absolute deviation is a result of the larger (more massive) drift gas, as the ion–neutral collision cross-section for any ion will increase in Ar relative to He. On the other hand, these data suggest the utility of multiple bath gases as a means of further confirming the presence of extended structure in gas-phase peptides. Repeated measurements of the same relative deviation for a specific peptide in a variety of drift gases increase the confidence level of ion mobility-based structural assignments. In addition, the apparent change in drift time profile for signal **III** suggests that some conformational selectivity could be gained through the optimization of drift gas parameters, especially polarizability. This observation is consistent with recent studies by Kohtani and Jarrold on the preference of certain conformational forms to interact with water in the gas phase.[31] The results of this study suggest that peptides containing a higher than average degree of secondary structure in the gas phase (such as signal **II**) are less susceptible to ion–neutral interaction than peptides that are more random coil (such as signals **I** and **III**).

There are also differences between the four overlaid plots in Plate 2 in terms of the number and identity of the signals observed as a function of drift gas. For example, we observed 18 signals for the aldolase digest (Plate 2) when using helium buffer gas and 26 or 29 signals for the same digest run under similar conditions utilizing methane or nitrogen as a buffer gas, respectively. At present, the source of this increase is not completely understood, and is the subject of continuing investigation.[38] There are several known processes that could lead to changes in the number of signals observed. For example, we have observed an increase

Table 1. Summary of peak capacity calculations for the four drift gases used

	Helium	Methane	Nitrogen	Argon
Nominal mass	4	16	28	40
Polarizability ($\times 10^{-24}$ cm^3)	0.20	2.60	1.73	1.62
No. of proteins digested	13	15	15	14
No. of peptides identified	234	462	366	150
Regression coefficient, average	0.998	0.98	0.98	0.98
Slope, average	0.25	0.33	0.39	0.52
Deviation, average (%)	±2.5	±3.0	±2.7	±1.7
Deviation, range (%)	+11.3 to −11.5	+13.6 to −11.6	+12.2 to −11.9	+6.5 to −9.0
Peak capacity, average[a]	1260	1650	1700	1190
Peak capacity, range[a]	5750	6920	7580	5430

[a] Calculated for an *m/z* range of 500–3500.

of in-source fragmentation of peptide ions using higher mass drift gases, such as Ar. It has also been observed that there is a decrease in ion suppression effects for MALDI ionization performed at higher pressure,[16] a finding that may also be altered with drift gas.

A summary of peak capacity calculations and regression parameters is presented in Table 1. Peak capacity calculations, utilizing the deviations for separate linear fits for each protein digest, show that the maximum peak capacity varies to a small degree as the polarizability of the drift gas is changed, ranging from $\phi = 5430$ for Ar to 7580 for N_2. However, the differences observed here are within the error of the peak capacity calculations, indicating that the estimate of ϕ for peptides is equivalent for the drift gases used in this study. Note that the decrease in peak capacity observed for peptide separation in argon relative to the other three datasets presented is supported by the higher degree of linear mass–mobility correlation observed for this dataset in Figs 2 and 3. This apparent decrease is not necessarily due to the relative ineffectiveness of IM separation in argon to disperse ions in 2-D space; it is more likely due to the limited mass range of peptides observed in the argon dataset, which presents an additional aspect to the peak capacity estimates made here. In order to be an effective measure of the separation abilities of a technique, the estimates made in this work are reflective not only of the separation method used, i.e. issues of orthogonality, but also the limit of detection of the technique. For example, a peptide separation method involving a massive (>40 u) but highly polarizable drift gas may be predicted (based on polarizability alone) to have a larger peak capacity than a He separation. However, based on the data presented in this paper, the ion transmission efficiency of the drift cell utilizing a massive drift gas may be poor enough to offset any peak capacity increase for complex peptide mixtures obtained through interaction potential.

CONCLUSIONS

The data presented here illustrate the limited utility of polarizability as a means of inducing differences in sequence selectivity and in the peak capacity of IM-MS separation. This result is not surprising owing to the relatively weak nature of the ion–induced dipole interactions utilized here (<0.5 kJ mol^{-1}).[39] However, in a limited number of cases apparent conformational selectivity is observed. Given the relatively weak nature of an ion–induced dipole interaction, a stronger interaction potential, derived from drift gases with permanent dipoles or hydrogen bonding capability, could significantly increase the peak capacity. The data also suggest that the gas-phase structure of tryptic peptides is potentially more complex than simple distinctions between random coil and recognizable secondary structure, as is indicated by the differences in drift time profile as a function of drift gas employed for signals **I** and **III** in Plate 2 (both identified as random coil). The results presented here illustrate that although the optimization of ion–neutral interaction can potentially lead to increased peak capacity, the choice of an optimized drift gas (or drift gas mixture) must strike a balance between interaction potential and transmission efficiency for the analysis of complex peptide mixtures. Future research in our laboratory in this area will involve the use of both stronger interaction potentials (ion–dipole and hydrogen bonding) along with decreased temperature (which should also increase the influence of ion–neutral interaction on the collision cross-section) and decreased field strength in an attempt to maximize IM-MS peak capacity for peptide separation.

Acknowledgements

Funding for this research was provided by the National Science Foundation (CHE-9629966), the Department of Energy, Division of Chemical Sciences, BES (DE-FG03-95ER14505) and the Texas Advance Research Program/Advanced Technology Program (TARP/ATP, 010366-0064-2001).

REFERENCES

1. Cheng X, Hochlowski J. Current application of mass spectrometry to combinatorial chemistry. *Anal. Chem.* 2002; **74**: 2679.
2. Aebersold R, Goodlett DR. Mass spectrometry in proteomics. *Chem Rev.* 2001; **101**: 269.
3. Kelleher NL. From primary structure to function: biological insights from large-molecule mass spectra. *Chem. Biol.* 2000; **7**: R37.
4. Burlingame AL, Carr SA, Baldwin MA (eds). *Mass Spectrometry in Biology and Medicine*. Humana Press: Totowa, NJ, 2000; 577.
5. MacCoss MJ, Wu CC, Yates JR. Probability-based validation of protein identifications using a modified SEQUEST algorithm. *Anal. Chem.* 2002; **74**: 5593.

6. Jensen ON, Podtelejnikov AV, Mann M. Identification of the components of simple protein mixtures by high-accuracy peptide mass mapping and database searching. *Anal. Chem.* 1997; **69**: 4741.
7. Griffin PR, Coffman JA, Hood LE, Yates JR. Structural analysis of proteins by capillary HPLC–electrospray tandem mass spectrometry. *Int. J. Mass Spectrom. Ion Processes* 1991; **111**: 131.
8. Peng J, Gygi SP. Proteomics: the move to mixtures. *J. Mass Spectrom.* 2001; **36**: 1083.
9. Champion MM, Campbell CS, Siegele DA, Russell DH, Hu JC. Proteome analysis of *Escherichia coli* K-12 by two-dimensional native-state chromatography and MALDI-MS. *Mol. Microbiol.* 2003; **47**: 383.
10. Wolters DA, Washburn MP, Yates JR. An automated multidimensional protein identification technology for shotgun proteomics. *Anal. Chem.* 2001; **73**: 5683.
11. Holland JF, Enke CG, Allison J, Stults JT, Pinkston JD, Newcome B, Watson JT. Mass spectrometry on the chromatographic time scale: realistic expectations. *Anal. Chem.* 1983; **55**: 997A.
12. Von Helden G, Wyttenbach T, Bowers MT. Conformation of macromolecules in the gas phase: use of matrix-assisted laser desorption methods in ion chromatography. *Science* 1995; **267**: 1483.
13. Jarrold MF. Peptides and proteins in the vapor phase. *Annu. Rev. Phys. Chem.* 2000; **51**: 179.
14. Hoaglund-Hyzer CS, Counterman AE, Clemmer DE. Anhydrous protein ions. *Chem. Rev.* 1999; **99**: 3037.
15. Valentine SJ, Counterman AE, Hoaglund CS, Reilly JP, Clemmer DE. Gas-phase separations of protease digests. *J. Am. Soc. Mass Spectrom.* 1998; **9**: 1213.
16. Ruotolo BT, Gillig KJ, Stone EG, Russell DH, Fuhrer K, Gonin M, Schultz JA. Analysis of protein mixtures by matrix-assisted laser desorption ionization–ion mobility–orthogonal time-of-flight mass spectrometry. *Int. J. Mass Spectrom.* 2002; **219**: 253.
17. Ruotolo BT, Verbeck GF, Thomson LM, Woods AS, Gillig KJ, Russell DH. Distinguishing between phosphorylated and nonphosphorylated peptides with ion mobility-mass spectrometry. *J. Proteome Res.* 2002; **1**: 303.
18. Stone EG, Gillig KJ, Ruotolo B, Fuhrer K, Gonin M, Schultz A, Russell DH. Surface-induced dissociation on a MALDI–ion mobility–orthogonal time-of-flight mass spectrometer: sequencing peptides from an 'in-solution' protein digest. *Anal. Chem.* 2001; **73**: 2233.
19. Stone EG, Gillig KJ, Ruotolo BT, Russell DH. Optimization of a matrix-assisted laser desorption ionization–ion mobility–surface-induced dissociation–orthogonal time-of-flight mass spectrometer: simultaneous acquisition of multiple correlated MS1 and MS2 spectra. *Int. J. Mass Spectrom.* 2001; **212**: 519.
20. Fuhrer K, Gonin M, McCully MI, Egan T, Ulrich SR, Vaughn VW, Burton WD, Schultz JA, Gillig K, Russell DH. Monitoring of fast processes by TOFMS. In *Proceedings of the 49th ASMS Conference on Mass Spectrometry and Allied Topics*, Chicago, IL, 2001.
21. Ruotolo BT, Gillig KJ, Stone EG, Russell DH. Peak capacity of ion mobility mass spectrometry: separation of peptides in helium buffer gas. *J. Chromatogr. B* 2002; **782**: 385.
22. Asbury GR, Hill HH. Using different drift gases to change separation factors (α) in ion mobility spectrometry. *Anal. Chem.* 2000; **72**: 580.
23. Matz LM, Hill HH, Beegle LW, Kanik I. Investigation of drift gas selectivity in high resolution ion mobility spectrometry with mass spectrometry detection. *J. Am. Soc. Mass Spectrom.* 2002; **13**: 300.
24. Beegle LW, Kanik I, Matz L, Hill HH. Effects of drift-gas polarizability on glycine peptides in ion mobility spectrometry. *Int. J. Mass Spectrom.* 2002; **216**: 257.
25. Hill HH, Hill CH, Asbury GR, Wu C, Matz LM, Ichiye T. Charge location on gas phase peptides. *Int. J. Mass Spectrom.* 2002; **219**: 23.
26. Mason EA, McDaniel EW. *The Mobility and Diffusion of Ions in Gases*. Wiley: New York, 1973; 384.
27. Mason EA. In *Plasma Chromatography*, Carr TW (ed). Plenum Press: New York, 1984; 43.
28. Boehringer H, Fahey DW, Lindinger W, Howorka F, Fehsenfeld FC, Albritton DL. Mobilities of several mass-identified positive and negative ions in air. *Int. J. Mass Spectrom. Ion Processes* 1987; **81**: 45.
29. Tammet H. Size and mobility of nanometer particles, clusters and ions. *J. Aerosol Sci.* 1995; **26**: 459.
30. Mesleh MF, Hunter JM, Shvartsburg AA, Schatz GC, Jarrold MF. Structural information from ion mobility measurements: effects of the long-range potential. *J. Phys. Chem.* 1996; **100**: 16 082.
31. Kohtani M, Jarrold MF. The initial steps in the hydration of unsolvated peptides: water molecule adsorption on alanine-based helices and globules. *J. Am. Chem. Soc.* 2002; **124**: 11 148.
32. Gillig KJ, Ruotolo BT, Stone EG, Russell DH. Periodic field focusing ion mobility spectrometer/mass spectrometer. *Rev. Sci. Instrum.* submitted.
33. Park ZY, Russell DH. Thermal denaturation: a useful technique in peptide mass mapping. *Anal. Chem.* 2000; **72**: 2667.
34. Giddings JC. Two-dimensional separations: concept and promise. *Anal. Chem.* 1984; **56**: 1258A.
35. Karger BL, Snyder LR, Horvath C. *An Introduction to Separation Science*. Wiley–Interscience: New York, 1973; 624.
36. Valentine SJ, Counterman AE, Hoaglund-Hyzer CS, Clemmer DE. Intrinsic amino acid size parameters from a series of 113 lysine-terminated tryptic digest peptide ions. *J. Phys. Chem. B* 1999; **103**: 1203.
37. Ruotolo BT, Verbeck GF, Thomson LM, Gillig KJ, Russell DH. Observation of conserved solution-phase secondary structure in gas-phase tryptic peptides. *J. Am. Chem. Soc.* 2002; **124**: 4214.
38. McLean JA, Ruotolo BT, Gilllig KJ, Russell DH. Enhanced protein coverage in peptide mass mapping with MALDI–ion mobility–TOF MS using alternate drift gases. *J. Proteome Res.* in preparation.
39. Böttcher CJF, Bordewijk P. *Theory of Electric Polarization*, (2nd edn), vol. 2. Elsevier: New York, 1978; 561.